A distinct class of hematopoietic stem cells develop from the human yellow bone marrow

Tammy T. Nguyen[1,2,5], Zinger Yang Loureiro[3,4], Anand Desai[4], Tiffany DeSouza[4], Shannon Joyce[4], Lyne Khair[1,2], Amruta Samant[1,2], Haley Cirka[2], Javier Solivan-Rivera[3,4], Rachel Ziegler[4], Michael Brehm[2,3,4], Louis M. Messina[1,2], Silvia Corvera[2,3,4,5]

[1]Department of Surgery, Division of Vascular Surgery, UMass Memorial Medical Center

[2]Diabetes Center of Excellence, UMass Chan Medical School

[3]Morningside Graduate School of Biomedical Sciences, UMass Chan Medical School

[4]Program in Molecular Medicine, UMass Chan Medical School

[5]Co-senior, co-corresponding authors at: silvia.corvera@umassmed.edu

Program in Molecular Medicine

373 Plantation Street

Worcester, MA 01605

ABSTRACT

Aging and metabolic diseases are accompanied by systemic inflammation, but the mechanisms that induce this state are not known. We developed a human bone-marrow organoid system to explore mechanisms underlying metabolic-disease associated systemic inflammation. We find that a distinct type of hematopoietic stem cell (HSC) develops in the adipose-rich, yellow bone marrow, which is known to gradually replace the hematopoietic red marrow as we age and during metabolic disease. Unlike HSCs derived from the red bone marrow, HSCs derived from the yellow bone marrow have higher proliferation rates, increase myeloid differentiation, skew towards pro-inflammatory M1 macrophage differentiation, and express a distinct transcriptomic profile associated with responsiveness to wounding. Yellow marrow-derived HSCs express higher levels of the leptin receptor, which we find to be further increased in patients with type 2 diabetes. Our work demonstrates that the human long bone yellow marrow is a niche for a distinct class of HSCs which could underlie hematopoietic dysfunction during aging and metabolic disease processes suggesting a shared inflammaging mechanism.

MAIN

The human bone marrow is a dynamic organ that is divided into two anatomic compartments; the red bone marrow provides the major hematopoietic stem cell (HSC) niche necessary for blood cell production, whereas the yellow bone marrow is a niche enriched in adipose tissue. The yellow marrow is first detected in the distal region of long bones by the age of seven, and progressively occupies more space within the long bone [1]. Conversely, the red marrow, an adipocyte poor tissue, occupies less space within the adult long bone and is gradually constrained

47 to the more proximal bone epiphyses during ageing[1,2]. The size of the yellow marrow is also
48 associated with several cancers, cardiovascular disease, and metabolic disease[3-9].
49
50 Aging is associated with increased HSC proliferation and myeloid-bias differentiation, which can
51 lead to hematopoietic dysfunction characterized by declining immune function [10-14]. A similar
52 pattern of increased HSC proliferation and myeloid-bias differentiation is observed during
53 systemic chronic inflammation[15-18]. Given that aging and chronic inflammatory diseases are
54 associated with expansion of the yellow bone marrow, we hypothesize that the yellow bone
55 marrow niche might promote inflammaging by promoting a hematopoietic process distinct from
56 that occurring in the red bone marrow niche.
57
58 Previously our laboratory developed a 3-dimensional (3D) *in vitro* organoid culture system to
59 study mechanisms of human adipose tissue development and function[19,20]. In this system, small
60 fragments of adipose tissue are embedded in a 3D hydrogel and cultured under conditions that
61 support angiogenesis from existing microvessels[19-21]. The development of new angiogenic
62 sprouts is accompanied by proliferation of mesenchymal progenitor cells, which remain in tight
63 association with developing vessels. Expanded progenitor cells maintain multipotency and the
64 capacity to differentiate into mesenchymal cell fates, including diverse adipocyte subtypes[22]. To
65 gain insight into the function of human red and yellow bone marrow niche on hematopoiesis, we
66 adapted this method to generate human bone marrow organoids from a diverse set of donors,
67 with the aim of understanding the complex interactions between HSC and mesenchymal
68 progenitor cells from two different bone marrow compartments that may differentially impact
69 human hematopoiesis[3,23,24].

70

71 We found that red marrow organoids generated from the trabecular epiphyseal region of the bone
72 and yellow bone marrow generated from the adipose rich diaphyseal region of the bone gave rise
73 to both mesenchymal progenitor cells and HSCs. HSCs did not develop from subcutaneous
74 adipose tissue outside the bone, demonstrating their specific location to the bone marrow niche.
75 HSCs from both red and yellow marrow could differentiate down the erythroid and myeloid
76 lineages and give rise to M1 and M2 macrophages. Unexpectedly HSCs from the yellow
77 marrow demonstrate a higher proliferation and differentiation rate when compared to HSCs
78 derived from the red marrow. Bulk and single-cell RNASeq reveal differences between both
79 mesenchymal progenitor cells and HSCs derived from red and yellow marrow organoids, that
80 point to distinct functional roles of hematopoiesis within each niche. These differences are
81 confirmed by direct analysis of excised bone marrow tissues. Moreover, these niche-specific
82 functions vary in subjects with or without type 2 diabetes. The technologies described provide a
83 new approach to advance the study of hematopoiesis and identify the human BMAT distinct
84 bone marrow niche for stress hematopoiesis with potential clinical impact.

85

86

87 **RESULTS**

88

89 **Expansion of Human Bone Marrow Hematopoietic Stem Cell Types from Anatomically**
90 **Distinct Niches.**

91

92 To explore the functional role of human bone marrow compartments, the red marrow (BMR), an
93 adipocyte poor tissue located at the proximal epiphysis of the adult long bone, and yellow
94 marrow (BMY), an adipocyte rich tissue located at the diaphysis of the adult long bone, were
95 collected alongside subcutaneous lower limb adipose tissue (BMS) from a diverse cohort of adult
96 donors (Fig. 1a-b, Extended Data Fig. 1a). Adipose tissue harvested from BMS and BMY have
97 similar unilocular adipocyte structure characteristic of white adipose tissue. Regions containing
98 small, dense nucleated cells were observed between adipocytes in BMY, but not in BMS, and
99 less frequently in BMR (Fig. 1c).
100
101 In order to expand these bone marrow niches, we embedded small fragments of BMS, BMY, and
102 BMR in MatriGel and cultured them under pro-angiogenic conditions[19,21]. *De novo* cell sprouting
103 was observed from all three tissue depots collected from seven different donors (Fig. 1d,
104 Extended Data Fig. 1b). After 14 days in culture, sprouting cells were recovered using Dispase
105 and Collagenase Type I. The cell number recovered was significantly higher from BMS
106 organoids in comparison to those derived from either bone marrow compartment, and similar
107 numbers of cells were recovered from BMY and BMR (Fig. 1e).
108
109 After plating in plastic, cells from all three depots had primarily a fibroblastic phenotype
110 characteristic of mesenchymal progenitor cells. Interestingly, BMY and BMR also gave rise to
111 small circular cells that resemble hematopoietic stem cells (HSC). These cells were not generated
112 by BMS-derived organoids (Fig. 1f). To test whether these small circular cells derived from
113 BMY and BMR truly represent HSC populations, we tested whether their expansion would be
114 stimulated by adding stem cell factor (SCF), interleukin-6 (IL-6), thyroperoxidase (TPO), Fms-

115 like tyrosine kinase 3 ligand (Flt3), pyrimido-indole derivative (UM171 or UM729), and
116 StemRegenin (SR-1)[25-27]. The addition of these cytokines and small molecule stimulators for
117 HSC expansion increased the frequency of small round cells with morphological features of
118 HSCs, whiles not significantly affecting total cell growth (Fig. 1 g-h, Extended Data Fig. 1c-d).
119
120 Cells harvested from BMS, BMY, and BMR organoids were probed for HSC cell surface
121 markers ($CD34^+$, $CD38^-$, $CD90^+$, $CD45^{low}$) (Fig. 1i), using human umbilical cord blood (HUCB)
122 as a control. Cells with HSC surface markers expanded from BMR and BMY organoids and
123 from HUCB, but not from BMS organoids, and the relative number of HSCs expanded from
124 BMY was higher compared to BMR (Fig. 1j, Extended Data Fig. 1e-f). These unexpected
125 results demonstrate that HSCs are present in the two anatomically distinct bone marrow
126 compartments: BMR and BMY. Moreover, the expansion of HSCs from BMY was more robust
127 than from the BMR niche, suggesting that bone marrow adipose tissue may differentially
128 enhance human hematopoiesis.
129
130 **Functional Differences Between Human Hematopoietic Stem Cells Derived from the Red**
131 **and Yellow Bone Marrow Niches**
132
133 To directly compare the functional properties of cells derived from BMS, BMY, and BMR
134 organoids, we isolated $CD34^+$ cells using an enrichment bead purification method (Fig. 2a). The
135 $CD34^+$ enriched cells from BMY and BMR were small and circular, similar in size and shape as
136 HSCs derived from HUCB controls, suggesting that both are functional HSC niches (Fig. 2b-c,
137 Extended Data Fig. 2a-b). We then tested whether $CD34^+$ cells were indeed functional HSCs

138 through colony forming unit assays. $CD34^+$ cells from BMY, BMR, or HUCB formed both
139 erythroid and myeloid colonies, whereas $CD34^+$ cells from BMS formed neither (Fig. 2d).
140 Significantly, BMY yielded a higher number of erythroid and myeloid colonies per number of
141 $CD34^+$ cells compared to BMR (Fig. 2e, Extended Data Fig. 2c-d).
142
143 To further determine the myeloid differentiation capacity of $CD34^+$ progenitor cells expanded
144 from BMY and BMR, we induced differentiation into downstream monocytes and macrophages.
145 Isolated $CD34^+$ progenitor cells from BMY, BMR, and HUCB cultures were induced into
146 monocyte differentiation with Monocyte Colony Stimulating Factor (M-CSF) and subsequently
147 induced into either pro-inflammatory M1 macrophage or anti-inflammatory M2 macrophage
148 with exposure to interferon gamma (IFNγ) or interleukin 4 (IL-4) and interleukin 13 (IL-13),
149 respectively (Fig. 2f). We observed that $CD34^+$ cells from both human red and yellow bone
150 marrow tissue can be induced towards monocyte and macrophage differentiation *in vitro*
151 similarly to $CD34^+$ cells from HUCB (Fig. 2g-h). Interestingly, we observed a reduction in anti-
152 inflammatory M2 macrophage differentiation among monocytes derived from BMR or BMY in
153 comparison to HUCB, and further reduction in BMY compared to BMR. The overall decrease in
154 anti-inflammatory M2 macrophage differentiation observed in bone marrow derived monocytes
155 may be donor source related, such as age (Extended Data Fig. 2e). M1 pro-inflammatory
156 macrophage differentiation from $CD34^+$ cells were similar when comparing cells derived from
157 either BMY, BMR or HUCB. Taken together, $CD34^+$ cells derived from BMY can form
158 erythroid and myeloid cells, and differentiate into monocytes and macrophages, similarly to
159 $CD34^+$ cells derived from BMR. However, $CD34^+$ cells derived from BMY have an increased
160 frequency of erythroid and myeloid colony formation when compared to BMR and trend towards

161 decreased anti-inflammatory M2 differentiation. These differences observed between $CD34^+$
162 cells derived from BMY and BMR may reflect specialized functional differences between these
163 two distinct bone marrow niches.
164
165 **Differential Features of the Human Yellow and Red Bone Marrow Niches**
166
167 To better understand the characteristics of the BMR and BMY niches, and how they may impact
168 hematopoiesis, we conducted bulk RNASeq of cells derived from BMS, BMY, and BMR
169 organoids cultured in the absence or presence of HSC cytokine stimulating media. Despite the
170 diversity of the patient cohort, varying in sex, age, race, and co-morbidities, the major difference
171 between differentially expressed genes among samples seen in principal component analysis
172 (PCA) was attributable to the depot of origin, with greatest differentially expression gene
173 variance between BMS and BMY+BMR (Fig. 3a). Similar clustering was observed for cells
174 grown in the presence of HSC cytokine stimulating media (Extended Data Fig. 3a). Moreover,
175 the addition of HSC stimulating cytokines and small molecules enhanced the expression of
176 hematopoietic genes in both BMR and BMY (Extended Data Fig. 3b-c). Samples from BMY and
177 BMR clustered more closely together than to BMS, and samples derived from BMY were more
178 dispersed in comparison to BMR and BMS, suggesting that BMY may be more sensitive to
179 donor-specific variables. Strikingly, pathway enrichment analysis of differentially expressed
180 genes between BMY and BMS cells revealed enrichment of immune and hematopoietic
181 regulatory pathways in the yellow bone marrow (Fig. 3b-c, Extended Data Fig. 3d). In contrast,
182 differentially expressed genes between BMR and BMS, cultured in either mesenchymal or HSC

183 cytokine stimulating media, were enriched in bone developmental pathways (Fig. 3d-e Extended
184 Data Fig. 3f).
185
186 Specific transcripts enriched in cells derived from BMY and associated with immune and
187 hematopoietic regulatory pathways included *DYNC1I1* (cytoplasmic subunit of dynein associated
188 with B-cell antigen presentation[28]); *PLA2R1* (phospholipase A2 receptor that regulates cytokine
189 production[29]); *LFNG* (lunatic fringe is a signaling regulator for T-cell differentiation[30]); *CD4* (
190 cluster of differentiation 4, marker for lymphocyte); *PGF* (placental growth factor, stimulator for
191 angiogenesis and bone marrow derived myeloid cell mobilization[31]); *CYBB* (component for
192 NADPH oxidase, loss of function in $CD34^+$ HSCs results in X-linked chronic granulomatosis[32]);
193 and *LEPR* (leptin receptor, associated with hematopoiesis and long-term engraftment[33-36]) (Fig.
194 3b-c). Specific transcripts associated with bone developmental pathways enriched in cells
195 derived from BMR included *BGLAP* (osteocalcin hormone, secreted by osteoblasts); *DLX5* and
196 *DLX6* (distal-less homeobox 5 and 6, regulators of osteogenesis[37]); *SP7* (transcription factor
197 required for osteocyte maturation[38]); *BMP3* (bone morphogenic protein 3, a negative regulator of
198 bone density[39]); and *WISP3* (Wnt1-inducible signaling protein 3, associated with a human
199 autosomal recessive skeletal disease, progressive pseudorheumatoid dysplasia[40]) (Fig. 3d-e).
200
201 More pronounced differences and enrichment in genes associated with immune and
202 hematopoietic regulatory pathways were seen upon direct comparison between BMY and BMR
203 (Fig. 3f). This comparison revealed increased expression in BMY of *EMCN* (endomucin, a
204 marker for endothelial cells and HSCs); *CD93* (cluster of differentiation 93, a marker for B cell
205 differentiation and quiescent and immature HSCs[41-44]); *LBP* (inflammatory modulatory

206 lipopolysaccharide binding protein [45]); *CD36* (cluster of differentiation 36, facilitates fatty-acid
207 uptake and oxidation and linked to HSC stress-induced expansion[46,47]); *SYK* (spleen tyrosine
208 kinase, critical in immune signaling [48]); *ITGAM* (integrin alpha-1, required for HSC
209 expansion[49]); *ITGAX* (also known as CD11c/CD18, a leukocyte adhesion molecule that regulates
210 stress-induced HSC expansion[50]); *SIGLEC9* (sialic acid binding Ig-like lectin 9, expressed on
211 immune cells and facilitate cell-cell interaction[51]); *NFAM1* (nuclear factor of activated T cells
212 activating molecule 1, an immunoreceptor that regulates T and B cell development[52]); and
213 *CXCL12* (CXC motif chemokine ligand 12, associated with quiescent HSC population
214 maintenance[53]) (Fig. 3f). These findings of immune cell development and hematopoiesis in
215 yellow bone marrow-derived organoids were unexpected since previous reports have ascribed
216 these functions primarily to the red marrow, whereas the yellow marrow is described primarily
217 as comprised of adipocytes and mesenchymal progenitors[3,24,54].
218
219 A key question raised by these findings is the extent to which BMY and BMR organoids reflect
220 the *in vivo* structural and functional features of the bone marrow. To address this question, we
221 performed bulk RNASeq on freshly excised BMS, BMY and BMR tissues, and compared their
222 transcriptomic profiles to determine whether differences between BMY and BMR organoids
223 would reflect *in vivo* features. Pathway enrichment analysis of genes differentially expressed
224 between excised tissues demonstrated enhanced immune and hematopoietic regulatory pathways
225 in BMY, and enhanced bone developmental pathways in BMR, similar to that found when
226 comparing cells from BMS, BMY, and BMR organoids (Fig. 3g, h and Extended Data Fig. 3h).
227 The similarities found between the transcriptomic profiles of BMS, BMY, and BMR tissues and

228 their respective organoids indicates that this system reflects *in vivo* physiology and comprises a
229 valid translational research model.
230
231 **Distinct Single-cell Transcriptomes from Red and Yellow Bone Marrow Niches**
232
233 To identify the cell types driving the distinguishing features of the BMY and BMR
234 hematopoietic niches, we performed single cell RNA sequencing. 9,376 cells derived from BMS,
235 9,691 cells derived from BMY, and 16,505 cells derived from BMR were collected. After
236 filtering out cells with low total sequencing count, high mitochondrial gene expression, and poor
237 nuclear cell lysis, 8,688 cells derived from BMS, 3,974 cells derived from BMY, and 12,307
238 cells derived from BMR remained and were used for subsequent data analysis (Extended Data
239 Fig. 4a-d). Based on Uniform Manifold Approximation and Projection (UMAP), progenitor
240 cells from BMS organoids have distinct expression profiles compared to those from BMR and
241 BMY. We observed some overlap in expression signatures between cells derived from BMY and
242 BMR , but, consistent with our bulk RNA sequencing data, the majority of cells derived are
243 distinct (Fig. 4a). The majority of cells derived from BMS, BMY, and BMR organoids expressed
244 mesenchymal progenitor cell markers, and few cells expressed CD34, the canonical marker for
245 HSCs (Fig. 4b-c). These results are concordant with FACS and functional data shown above
246 indicating the expansion of both mesenchymal progenitor cells and HSCs expanding from both
247 anatomically distinct human bone marrow niches.
248
249 Consistent with our findings from cell enrichment experiments (Fig. 4c, Fig. 2c, Extended Data
250 Fig. 4e), analysis of single-cell transcritomes indicates that $CD34^+$ cells represent 1.7% of the

251 BMS, 0.94% of the BMY, and 0.48% of the BMR organoid cell population. However, functional
252 HSCs, capable of differentiating into blood lineages, developed only from BMY and BMR, but
253 not from BMS. Morever, monocytes developing from BMY differentiate into higher proportion
254 of M1 macrophages. To identify genes associated with the observed functional properties of each
255 $CD34^+$ cell population, we performed pseudobulk analyses. When comparing $CD34^+$ cell
256 trancriptomes with those of all $CD34^-$ cells in the population, $CD34^+$ cells from BMY were the
257 most different, with 363 genes differentially expressed (log2 fold change >0.5) (Fig. 4d-e,
258 Extended Data Fig. 4f-g). These genes were enriched in pathways corresponding to wound
259 responsiveness and hypoxia (Fig. 4f-g), and included genes associated with hematopoiesis, such
260 as, *SPARCL1 (SPARC like 1,* an extracellular protein involved in cell migration)*; PECAM1*
261 *(*platelet endothelial cell adhesion molecule 1, a marker for HSC[55,56]); and *CXCL12*, (a ligand
262 associated with quiescent HSC population maintenance[53]) (Fig. 4d-e). In contrast, $CD34^+$ cells
263 from BMR are enriched for immune and skeletal development pathways (Extended Data Fig.
264 4g). These results verify the HSC features of $CD34^+$ cells derived from BMY and reinforces the
265 concept of the yellow bone marrow as a hematopoietic niche distinct from BMR.
266
267 To examine the features of the $CD34^-$, mesenchymal progenitor cell populations in each bone
268 marrow niche, we compared $CD34^-$ cells derived from BMY and BMR (Extended Data Fig. 4h-
269 i). This analysis revealed 334 genes with higher expression in cells from BMY and 113 genes
270 with higher expression in cells from BMR (log 2 fold change > 0.5). Pathway enrichment
271 analysis revealed that cells from BMY organoids were enriched in immune pathways, aging, and
272 bone development, with specific genes including *IGFBP5* and *IGFBP7* (insulin growth-like
273 factors binding proteins); *MGP* (matrix Gla protein, an inhibitor of vascular mineralization[57]);

274 *HGF* (hepatocyte growth factor, involved in HSC mobilization[58]); and *LEPR (*a tyrosine kinase
275 receptor associated with support of the HSC niche[34-36,57]) (Extended Fig. 4h). BMR CD34$^-$
276 progenitor cells are enriched in glycolytic and telomere regulatory pathways (Fig. 4f-g), with
277 specific genes including *SPPI or OPN (*osteopontin, a secreted phosphoprotein that functions in
278 bone homeostasis, regulation of primitive HSC at the endoseal niche, and age-related changes in
279 HSC function[59-61]); *SULF1* (sulfatase 1, fibroblast growth factor co-receptor involved in HSC
280 differentiation[62]); and *ID3* (inhibitor of DNA binding, a transcription factor binding protein
281 associated with maintaining the HSC sinusoidal niche homeostasis[63]) (Extended Fig. 4i). The
282 transcriptomic distinction between the human yellow and red bone marrow derived CD34$^-$
283 mesenchymal progenitor cells suggests that they may provide specialized niches for two
284 anatomically distinct HSC populations.
285
286 To obtain a holistic view of the potential function of each bone marrow niche, we searched for
287 pathways shared by both mesenchymal progenitors (CD34$^-$ cells) and HSCs (CD34$^+$ cells)
288 originating from the two bone marrow niches. Pathway analyses of genes differentially
289 expressed by CD34$^+$ cells between BMR and BMY, and of genes differentially expressed by
290 CD34$^-$ cells between BMR and BMY revealed a subset of biological pathways common to both
291 CD34$^+$ and CD34$^-$ cells within each bone marrow niche (Fig. 4f-g, Extended Data Fig. 4h-i). The
292 BMY niche is enriched in wound responsiveness and hypoxia pathways, with representative
293 genes including *LEPR*, *SOD2*, *ENG*, and *CXCL12* (Fig. 4h). In contrast, the BMR niche is
294 enriched in phosphorous metabolism, protein regulation, and vascular development pathways.
295 These data are consistent with a specific function for the BMY and BMR hematopoietic niches,
296 where the BMY niche is more sensitive to hypoxia and inflammatory processes.

297

298 **Differences in the Yellow Bone Marrow from Subjects with Chronic Diabetic Wounds**

299

300 To test the hypothesis suggested by pathway analyses that the BMY hematopoietic niche is
301 particularly responsive to hypoxia and inflammatory processes, we sought to determine whether
302 genes enriched in BMY differ between clinically different subjects. *LEPR* expression is
303 consistently higher in BMY when compared to BMR organoids (Fig. 5a) and is differentially
304 expressed in between the $CD34^+$ and $CD34^-$ cell populations (Fig. 5b). In mice LEPR has been
305 shown to be expressed on mesenchymal progenitor cells within the bone marrow and
306 hypothesized to maintain HSC quiescence in perivascular regions[17,34-36,64-68]. We first examined
307 whether differential expression of *LEPR* in BMY occurs *in vivo*, using BMS, BMY, and BMR
308 excised tissue. We detected *LEPR* expression in all donor samples (Fig. 5c, Extended Data Fig.
309 5a), with variability potentially attributable to donor specific variables including age, sex, race,
310 and diabetes status (Extended Data Fig.5b). We observed that *LEPR* transcript expression is
311 higher in BMY tissue compared to BMR tissue in donors with Type 2 diabetes. Moreover, we
312 also found a significant higher expression of *LEPR* in cells derived from BMY relative to BMR
313 organoids from donors with diabetes (Fig. 5d-e). These results are consistent with a distinct
314 functional role for the yellow marrow in hematopoiesis and in response to chronic inflammatory
315 disease.

316

317

318 **DISCUSSION**

319 The mechanisms for systemic inflammation associated with aging and metabolic diseases are
320 unknown. Both aging and metabolic diseases are associated with the phenotypic changes in the
321 bone marrow that may provide insight into the driving mechanisms for inflammaging. Several
322 studies have demonstrated a gradual expansion of the adipose-rich yellow bone marrow at the
323 expense of the trabecular bone red bone marrow niche during aging and metabolic diseases.[2,5,9,69]
324 However, the consequences of this dynamic change in the bone marrow on hematopoiesis and
325 stress response has not been systematically examined in humans. A major barrier to performing
326 comparative analysis between the red and yellow bone marrow niche is due to the fact that
327 obtaining cells from the adipocyte-rich bone marrow niche is technically fraught due to the
328 volume and fragility of adipocytes. In this study, we utilized a 3D organoid bone marrow culture
329 system to tested whether the yellow bone marrow niche might promote inflammaging by
330 promoting a hematopoietic process distinct from that occurring in the red bone marrow niche.
331
332 We developed a 3D organoid culture system to explore the respective properties of the red and
333 yellow human bone marrow niches. Using bulk RNA Seq and pathway enrichment analysis, we
334 find that cells expanded from organoids *in vitro* maintain distinct transcriptomic features found
335 *in vivo*, confirming the translational research potential of this approach. We found that expand
336 $CD34^+$ cells from BMY, despite vast differences among our donors' demographic phenotypes
337 (Extended Data Figure 2b), routinely resulted in a higher proportion of cells with canonical HSC
338 markers compared to BMR organoids (Fig. 1i-j). $CD34^+$ HSCs derived from the yellow marrow
339 could form erythroid and myeloid colonies more efficiently than those from the red marrow
340 under similar *in vitro* conditions (Fig. 2e). Intriguingly, the discovery of a relative increase in
341 $CD34^+$ HSC number with increased myeloid lineage differentiation from BMY mirrors the

342 hallmark phenotypes for aging HSCs and response to chronic low-grade infections.[11,14-16,70]
343 Given that aging is linked with expansion of the BMY niche and aging HSCs are accompanied
344 by reduced self-renewal ability, impaired homing, myeloid-biased differentiation, and clonal
345 expansion, it is possible that the BMY niche, unlike the BMR niche, is driving the age-related
346 dysfunctions in hematopoiesis.
347
348 The identification of functional HSCs within both anatomically distinct bone marrow tissues
349 suggest that there are two hematopoietic niches within the human long bone with potentially
350 distinct functions in human hematopoiesis. The transcriptomes of HSCs derived from the two
351 different niches reflect the BMY and BMR HSC functional differences. Enrichment analysis of
352 differentially expressed genes suggest distinct functions. For example, BMY-derived $CD34^+$
353 cells have an increased expression of *CD93*, a lectin-type transmembrane receptor important for
354 cell-to-cell adhesion and a marker for quiescent and immature HSCs [41-44], , as well as increased
355 expression of several extracellular adhesion proteins, such as SPARCL1, PECAM1, CLDN5,
356 and CXCL12 (Extended Data Fig. 4f). These features resemble those of quiescent and immature
357 HSC populations. Quiescent long-term HSCs can reconstitute the hematopoietic system
358 continuously, whereas short-term HSCs can sustain hematopoiesis for only a few weeks[54]. Aging
359 and chronic inflammation can lead to LT-HSCs increased myeloid-biased output, replicative
360 exhaustion, and poor response to infection.[13,70,71] It is intriguing to speculate whether HSCs in
361 BMY, which display enhanced expansion and erythroid and myeloid colony formation *in vitro*
362 may be enriched in a long-term HSC population that may be particularly sensitive to aging and
363 stress-response inflammation, such as in response to wounding (Fig. 4g-h).
364

365 Among the top differentially expressed genes in HSCs from the yellow marrow is the leptin
366 receptor (*LEPR*). *LEPR*$^{+}$ bone marrow cells have been reported to represent perivascular
367 mesenchymal progenitor cells important for HSC maintenance [34]. Moreover, we have previously
368 shown that *Lepr* knockout mice (Db/Db, mice) have delayed wound healing, and bone marrow
369 from *Lepr* knockout mice transplanted into wild-type mice is sufficient to impair wound healing
370 [72]. Notably, we find that *LEPR* expression is higher in both HSC and mesenchymal progenitor
371 cells derived from yellow marrow organoids. We verified that this enhanced expression seen *in*
372 *vitro* also occurs *in vivo*, as the relative expression of *LEPR* is higher in yellow compared to red
373 marrow tissue (Fig 5b). This difference is unlikely to be due to the presence of adipocytes in the
374 yellow marrow, as the expression of *LEPR* in vicinal subcutaneous adipose tissue was lower than
375 either of the two marrow niches. These data suggest that LEPR^{+} cells in the yellow marrow, both
376 MSCs and HSCs, may enhance active hematopoiesis during a stress response, such as wounding.
377
378 To further explore this hypothesis, we leveraged the diversity of our human cohort, which
379 includes diabetic donors with non-healing diabetic foot ulcers, to determine whether *LEPR*
380 expression in BMY is affected in diabetes. Not surprisingly, we found a wide variance in *LEPR*
381 expression between donors; nevertheless, when we normalized the expression of *LEPR* in the
382 BMY to that in the BMR niche within each donor we found a higher ratio in patients with
383 diabetes. These data are consistent with the hypothesis that the hematopoietic response within the
384 yellow bone marrow niche may specifically respond to stresses such as wounding and is
385 impacted by human metabolic disorders. Further experiments to directly examine the effects of
386 leptin on proliferation and function of HSCs and MSCs from human bone marrow niches will
387 help address this hypothesis.

388

389 In addition to HSCs, hematopoiesis requires support from multipotent mesenchymal progenitor
390 cells within the bone marrow. These cells act through secreted signaling factors and intercellular
391 communication within the niche. We find significant differences between mesenchymal
392 progenitor cell populations from the yellow and red bone marrow niches (Fig 3 and 4), where
393 cells from the yellow marrow are enriched in hematopoietic and immune pathways (Fig. 3c and
394 Extended Data Fig. 3d), while red marrow progenitor cells are enriched in bone developmental
395 pathways. These data suggest that yellow marrow mesenchymal cells may support active
396 hematopoiesis whereas red marrow mesenchymal cells may support maintenance of the
397 trabecular bone and less active hematopoiesis.

398

399 More granular differences between mesenchymal progenitor populations were seen through
400 scRNA Seq analysis of $CD34^-$ cells. Cells from BMY were enriched in genes implicated in
401 wound response pathways and responsiveness to low oxygen, while cells from BMR were
402 enriched in genes implicated in glycolytic pathways, presupposing a high oxygen environment
403 (Fig. 4f-g). Differences in oxygen tension are associated with distinct HSC subtypes, where early
404 hematopoietic progenitors with enhanced capacity for self-renewal reside in areas with low
405 oxygen tension, while areas of high oxygen tension are associated with increased mitochondrial
406 reactive oxygen species and depletion of the HSCs[73]. The transcriptomic features of MSCs from
407 the yellow marrow, suggestive of a low oxygen tension environment, are consistent with the
408 ability of this niche to maintain a quiescent HSC population with high capacity for self-renewal.
409 This enhanced capacity may explain our findings of increased proliferation and differentiation

410 exhibited by isolated $CD34^+$ cells expanding from the yellow marrow. In contrast, the red
411 marrow may be a high oxygen microenvironment that results in HSC depletion.
412
413 Our study is limited by several factors, the principal being the low number of amputees with or
414 without diabetes that can be reasonably compared given the large variation in factors such as age,
415 sex and other morbidities. We also recognize that we have not assessed the capacity of HSCs
416 from red and yellow marrow to reconstitute the immune system *in vivo*. This limitation will be
417 overcome with a better understanding of the variables that limit engraftment of HSCs after their
418 proliferation in culture, which is a known barrier in the field. The use of organoid cultures to
419 expand HSCs from bone marrow niches as well as from human umbilical cord provides a new
420 platform with which to address these outstanding questions. Despite these limitations, our results
421 strongly support that each bone marrow niche, BMR and BMY, play a distinct functional role in
422 hematopoiesis. Our technology helps overcome the paucity of information on the role of the
423 yellow marrow in humans, attributable to the general difficulties of studying adipocyte-rich
424 tissue, and to the difficulties in sourcing human bone marrow. Our results may help understand
425 the driving mechanisms for HSC dysfunction during inflammaging. Moreover, the identification
426 of the BMAT as a source of HSCs during stress conditions and metabolic disease may provide
427 potential clinical benefits for developing strategies to enhance effective hematopoiesis.
428
429
430 **METHODS**
431

432 ***Human Subjects:*** Lower extremity subcutaneous adipose tissue, yellow bone marrow adipose
433 tissue, and red marrow adipose tissue was collected from discarded tissue of patients undergoing
434 lower extremity amputation, with approval from the University of Massachusetts Institutional
435 Review Board (IRB H00020377).
436
437 ***Histology:*** All samples were fixed in 4% paraformaldehyde at 4ºC and thoroughly washed with
438 PBS and embedded in paraffin. Tissue sections (10 μm) were mounted on Superfrost Plus
439 microscope slides (Fisher Scientific) and stained with hematoxylin and eosin. Tissue sections
440 were imaged using ZEISS Axio Scan.Z1.
441
442 ***Generation of 3D tissue explant co-culture system:*** Methods for the harvesting and the culture
443 adipose tissue explants were previously published (Min, et al., 2016). Human tissues were
444 donated from consented adult patients undergoing lower extremity amputation surgery at
445 University of Massachusetts Medical Center and were subjected to harvesting within one to two
446 hours. Explants of approximately $1cm^3$ in size were embedded in Matrigel Matrix (Cat# 356231,
447 Corning) per 10 cm dish with EGM-2MV (Cat# CC-3156,CC-4147, Lonza) media
448 supplementation. The excised tissue was embedded in Matrigel (180 explants/10 cm dish) or (30
449 explants/6-well dish) and cultured for 14-17 days as described before. Addition of 100ng/mL
450 stem cell factor (SCF), 100ng/mL interleukin-6 (IL-6), 100ng/mL thyroperoxidase (TPO),
451 100ng/mL Fms-like tyrosine kinase 3 ligand (Flt3), 35mM pyrimido-indole derivative (UM171
452 or UM729), and 0.75 uM StemRegenin (SR-1) was added to culture to promote HSC expansion.
453 After 12-17 days in Matrigel, the progenitors in explants were recovered using Dispase (Cat#

454 354235, Corning) for one hour followed by additional 14 minutes of Trypsin-EDTA (Cat#
455 15400-054, Gibco) and Collagenase I (Cat# LS004197, Worthington).
456
457 ***RNA extraction and quantitative PCR:*** Cells were placed on TRIzol (Invitrogen) and
458 homogenized with Tissuelyser (Qiagen). Total RNA was reverse transcribed using the iScript™
459 cDNA Synthesis Kit (Cat# 1708891, Bio-Rad) per manufacturer's protocol. Quantitative reverse-
460 transcription PCRs were prepared with iQTM SYBR Green Supermix (Cat# 1708882, Bio-Rad)
461 and were performed on a CFX Connect Real-Time PCR Detection System (Bio-Rad).
462 Amplification of human-specific genes using the following primers:
463

Primers	Forward	Reverse
Human RPL4	GCC TGC TGT ATT CAA GGC TC	GGT TGG TGC AAA CAT TCG GC
Human LEPR	GCT ATT TTG GGA AGA TGT	TGC CTG GGC CTC TAT CTC

464
465 ***Bulk RNA-Seq:*** RNA was extracted from dispase cells using the TRIzol method. The cell-
466 TRIzol mixtures were transferred to collection tubes and homogenized with Tissuelyser II
467 (Qiagen). Chloroform was added in a 1:5 ratio by volume and phase separation was performed.
468 The RNA-containing layer was mixed with an equal volume of 100% isopropanol and incubated
469 overnight at -20 °C for precipitation. RNA was pelleted and washed with 80% ethanol and
470 resuspended in nuclease-free water. RNA concentration and purity were determined using a
471 NanoDrop 2000 (Thermo Scientific). RNA for sequencing were sent to University of
472 Massachusetts Medical School Molecular Biology Core Lab for fragment analysis.
473

474 Single-cell library preparation was performed using Chromium™ Single Cell 3' GEM Library &
475 Gel Bead Kit v3 (Cat# 1000092, 10X Genomics) according to manufacturer's instruction. The
476 libraries were sequenced on the NovaSeq system (Illumina) using the NovaSeq® 6000 S4 Kits
477 v1.5 (35 cycles; Cat# 20044417, Illumina) performed by Azenta Life Science. The generated
478 .fastq files were loaded into the DolphinNext platform (https://dolphinnext.umassmed.edu/) and
479 the Bulk RNA sequencing pipeline was used[74]. The .fastq files were aligned to the human (hg19)
480 genome and normalized by RSEM (v1.3.1)[75]. Differential expression analysis was performed
481 using the DEBrowser platform (https://debrowser.umassmed.edu/)[76]. Pathway analysis was
482 performed by combining the Gene ontology analysis (https://geneontology.org/) and TopFunn
483 (https://toppgene.cchmc.org/) results. Sequencing results were submitted to GEO (accession
484 number: GSE231377). Sequencing results and analysis scripts will be made publicly available
485 upon publication of the manuscript.
486
487 ***Single Cell RNA-Seq:*** Single-cell library preparation was performed using Chromium™ Single
488 Cell 3' GEM Library & Gel Bead Kit v3 (Cat# 1000092, 10X Genomics) according to
489 manufacturer's instruction. The libraries were sequenced on the NovaSeq system (Illumina)
490 using the NovaSeq® 6000 S1 Kits v1.5 (300 cycles; Cat# 20028317, Illumina) performed by
491 Azenta Life Science. The sequencing outputs were processed using the CellRanger software
492 v3.1.0 on the Massachusetts Green High Performance Computer Cluster (GHPCC). Reads were
493 mapped to human reference genome GRCh19 (Ensembl 19). Data analysis was performed using
494 Seurat v4.1.0 within R version 4.0.2 environment[77]. Sequencing results and analysis scripts will
495 be made publicly available upon publication of the manuscript.
496

497 ***CD34 Positive Cell Enrichment:*** CD34$^+$ cells were enriched from *de novo* progenitor cells
498 collected from each respective 3D hydrogel tissue explant culture using the EasySep Human
499 CD34 Selection (StemCell Technologies, #17856). HUCB CD34$^+$ cells were isolated from whole
500 blood using Lymphoprep (StemCell Technologies, #07801) to collect mononuclear cells then
501 purified using EasySep Human Cord Blood CD34 Selection (StemCell Technologies, #17896).
502 HUCB CD34$^+$ cells were then seeded in Matrigel Matrix (Cat# 356231, Corning) for 14-17 days
503 for HSC expansion. After HSC culture expansion, HUCB CD34$^+$ cells in Matrigel Matrix were
504 then harvested using Dispase (Cat# 354235, Corning) for 40 minutes followed by additional 14
505 minutes of Trypsin-EDTA (Cat# 15400-054, Gibco) and Collagenase I (Cat# LS004197,
506 Worthington). HUCB CD34$^+$ cells harvested from Matrigel Matrix were subsequently enriched
507 using EasySep Human Cord Blood CD34 Selection (StemCell Technologies, #17896). Enriched
508 CD34$^+$ were then either used for FACS, colony forming unit assay, or *in vitro* differentiation.
509
510 ***Colony Forming Unit Assay and Monocyte/Macrophage In Vitro Differentiation:*** Enriched
511 CD34$^+$ cells were resuspended to a final volume of 1.5 mL with semisolid Methocult (StemCell
512 Technologies, #04404) and then plated in 6-cm dishes and incubated at 37°C in 5% CO_2.
513 Between 6 and 14 days, the number of colony-forming unit-erythrocyte (CFU-E) and CFU-
514 granulocyte-erythrocyte-monocytes-macrophage (CFU-GEMM), were scored under a
515 microscope.
516
517 HSC expansion using isolated CD34$^+$ cells were cultured in StemSpan (StemCell Technologies,
518 #09645), 1% Pen/Strep, 50ng/ml SCF (PreproTech, # 300-07-10UG), 50ng/ml Flt3
519 (PrepreoTech, # 300-19-10UG), 20ng/ml TPO (PreproTech, # 300-18-10UG), 20ng/ml IL-6

520 (PreproTech, # 200-06-20UG), 0.75 uM StemRegenin 1 (SR1, StemCell Techologies, # 72342),
521 and 35nM UM729 (StemCell Technologies, # 72332). Monocyte differentiation was induced
522 from HSC for 5-7 days in RPMI (Gibco, #11875093), 10% FBS, 1% Pen/Strep, 50ng/mL SCF
523 (PreproTech, # 300-07-10UG), 50ng/ml Flt3 (PrepreoTech, # 300-19-10UG), 20ng/ml TPO
524 (PreproTech, # 300-18-10UG), 25ng/ml M-CSF (PreproTech, # 300-25-10UG). Inflammatory
525 M1 Macrophage differentiation was induced from monocytes for 24-36 hours in in RPMI
526 (Gibco, #11875093), 5% FBS, 1% Pen/Strep, and 100ng/mL IFNγ (PreproTech, # 300-02-
527 20UG). Anti-inflammatory M2 Macrophage differentiation was induced from monocytes for 24-
528 36 hours in in RPMI (Gibco, #11875093), 5% FBS, 1% Pen/Strep, and 10ng/mL IL-4
529 (PreproTech, # 200-04-5UG) and 10ng/mL IL-13 ((PreproTech, # 200-13-2UG).
530
531 ***Flow Cytometry:*** Flow cytometry assays were performed on BD LSR II A-5. Viable cells were
532 determined with live/dead cell marker (Invitrogen™ eBioscience™ Fixable Viability Dye
533 eFluor™ 455UV, ThermoFisher Scientific #65-0868-14). The following fluorescent conjugated
534 antibodies at a 1:50 dilution were used:
535

BioLegend Cat#	
348803	Human lineage APC
304023	Alexa Fluor 700™ anti-human CD45 Antibody
343605	PE anti-human CD34
356607	PE/Cy7 anti-human CD38
328107	FITC anti-human CD90 (Thy1)
305013	APC anti-human CD64
333611	Brilliant Violet 421 anti-human CD163
321120	APC-Cy7 anti-human CD206

367115	FITC anti-human CD14

536

537 Flow cytometry data analysis was performed with FACS Diva 6.1 software and analysis done on
538 FloJo software (10.8.1).

539

540 ***HSC-induced Differentiation Towards Monocytes and Macrophages***: CD34 positive cells
541 enriched using magnet beads (StemCell) were cultured in complete RPMI 1640 medium (10%
542 FBS, 100 U/ml penicillin, 100 U/ml streptomycin, with 50 ng/ml SCF, 20 ng/ml TPO, and 50
543 ng/ml Flt3 with 25 ng/ml M-CSF (Peprotech). After 5-7 days, cells were induced to differentiate
544 towards M1 macrophage by changing the medium to the M1 induction medium (complete RPMI
545 1640 medium, 5% FBS, 100 U/ml penicillin, 100 U/ml streptomycin, and 5 ng/mL IFN-gamma
546 for 24-36 hours. Cells were then collected and stained FACS analysis. Stained cells were run
547 through a BD FACSCalibur flow cytometer and data were analyzed using the FlowJo software
548 (VERSION). All the cytokines were purchased from Peprotech and all the antibodies were
549 purchased from BD Biosciences.

550

551 ***Statistical analysis:*** Statistical analyses were performed using GraphPad Prism 9.2. In analyses
552 where multiple groups were compared, a one-way or two-way parametric ANOVA was used
553 with subsequent adjustments for multiple comparisons. Two-tailed statistical tests were always
554 used. All exact P values <0.05 are shown.

555

556 **ACKNOWLEDGEMENTS**

557 This study was supported by NIH grants DK089101 and DK123028 to SC, Vascular and
558 Endovascular Society Early Career Award, Wylie Scholar Award, and 1K08DK134k52 to TTN.

We acknowledge the use of services from the following UMASS cores: Flow Cytometry Core, Molecular Biology Core, and Morphology Core.

AUTHOR CONTRIBUTIONS

TTN: hypothesis generation, conceptual design, experiment design and performance, data analysis, manuscript preparation. ZYL: conceptual design, experiment design and performance, data analysis, manuscript preparation. AD: experiment design and performance, data analysis, manuscript preparation. TD: experiment design and performance, data analysis, manuscript preparation. SJ: experiment design and performance, data analysis, manuscript preparation. SF: experiment design and performance, data analysis, manuscript preparation. LK: experiment design and performance, manuscript preparation. HC: experiment design and performance, data analysis, manuscript preparation. AS: experiment design and performance, manuscript preparation. JSR: conceptual design, manuscript preparation. MB: conceptual design, manuscript preparation. LMM: conceptual design. SC: supervision of work, hypothesis generation, conceptual design, manuscript preparation.

582 **FIGURES and LEGENDS**

583 **FIGURE 1**

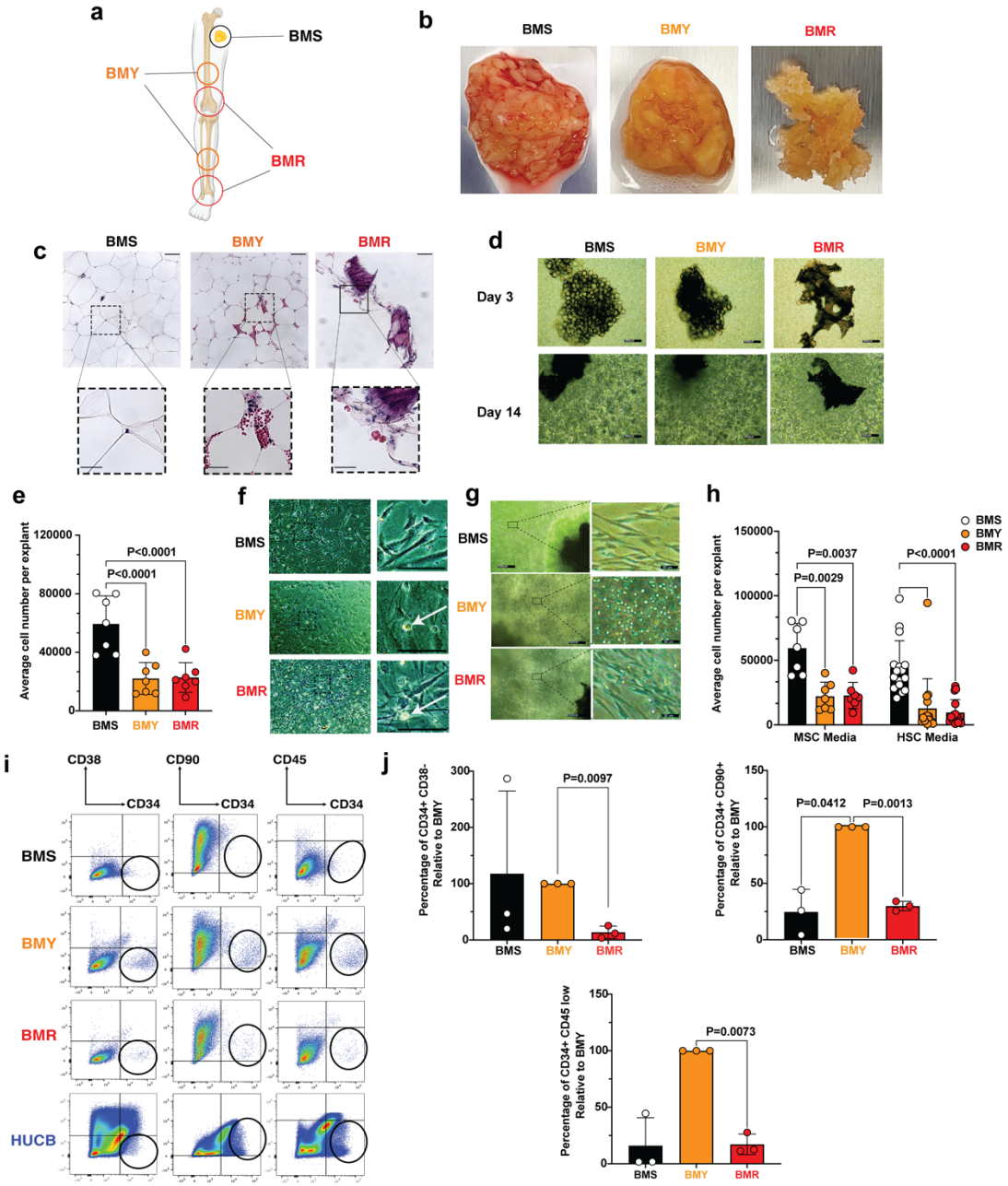

584

585 **Fig. 1. Hematopoietic stem cell expansion from human bone organoid cultures. a**)

586 Schematic of lower extremity bone with anatomic location of red marrow (BMR), yellow

587 marrow (BMY), and subcutaneous adipose tissue (BMS). **b**) Representative gross images of

588 harvested tissue from each depot. **c)** Representative hematoxylin and eosin image of harvested
589 tissue from each depot. Scale bar 200 μm. **d**) Representative images of BMS, BMY, and BMR
590 tissue after 3 days and 14 days in 3D organoid culture. Scare bar 500 μm. **e**) Average number of
591 cells per explant per tissue depot. Values are number of cells recovered divided by number of
592 explants seeded, for each of n=7 donors. Error bars = SD. Statistical significance was calculated
593 using ordinary 2-way ANOVA as implemented in GraphPad Prism v9.2, and exact P values are
594 shown. **f**) Representative images of cells harvested from organoid cultures after plating on
595 plastic. Arrows indicate circular round cells. Scale bar 100 μm. **g**) Representative images of
596 organoid cultures after 14 days under HSC medium. Scale bar 500 μm. **h**) Number of cells per
597 explant after 14 days of culture in mesenchymal (MSC) or hematopoietic (HSC) proliferative
598 media conditions. Values are number of cells recovered divided by number of explants seeded,
599 for each of n=7 and n=17 donors for MSC and HSC conditions. Error bars = SD, Statistical
600 significance was calculated using ordinary 2-way ANOVA. **i**) Representative FACS analysis of
601 cells generated from BMY and BMR organoids in comparison to HUCB cultured under identical
602 conditions. Cell populations circled express canonical HSC cell surface markers ($CD34^{+}CD38^{-}$,
603 $CD34^{+}CD90^{+}$, and $CD34^{+}CD45^{low}$). **j**) Quantification of cells positive for canonical HSC FACS
604 markers developing from BMS, BMY and BMR from n=3 donors. To correct for the variation in
605 the number of cells used for FACS for each donor, the number of cells from BMR and BMS is
606 expressed as a percent of the number of cells from BMY. Error bars = SD. Statistical
607 significance was calculated using ordinary 2-way ANOVA, and exact P values are shown.
608

609 **FIGURE 2**

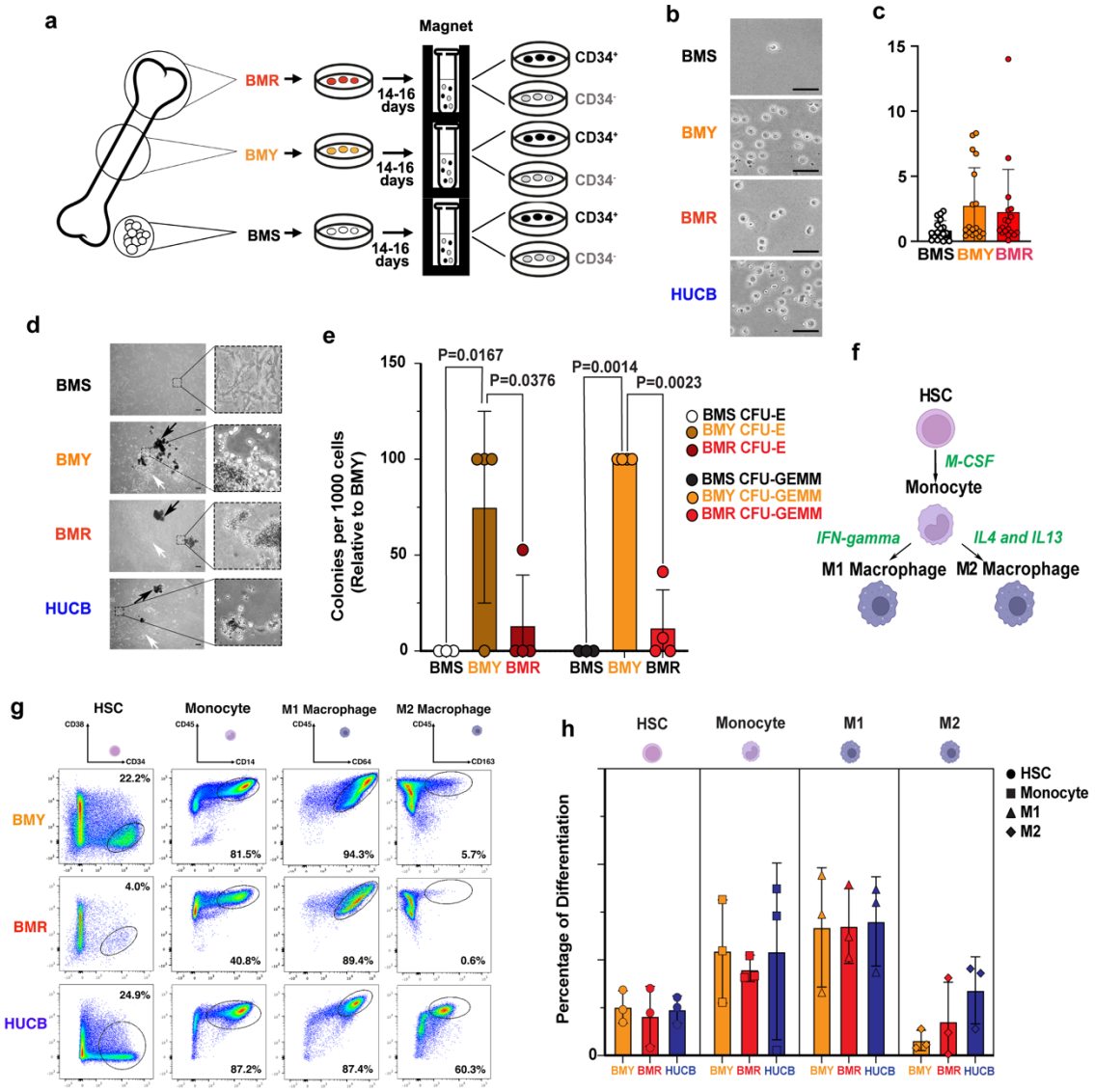

610

611 **Fig. 2. Similar functional properties of HSCs derived from red or yellow marrow. a)**

612 Schematic of process for collection of CD34+ cells, showing collection sites for BMS, BMY,

613 and BMR explants. After 14-16 days in 3D organoid culture, a single cell suspension is obtained

614 by enzymatic digestion and $CD34^+$ cells purified using antibody coated magnetic beads. **b)**

615 Representative images of $CD34^+$ cells purified from BMS, BMY, BMR, and HUCB. Scale bar =

616 100µm. **c)** Number of $CD34^+$ cells obtained from BMS, BMY, BMR, expressed as percent of

617 total single cells. **d**) Representative images of colony forming units formed by $CD34^+$ cells
618 derived from BMS, BMY and BMR tissue explants or HUCB. Black arrows indicate erythroid
619 colonies and white arrows indicate myeloid colonies. Scale bar =10μm. **e**) Comparison of
620 colony forming units per thousand $CD34^+$ cells, where BMY is set to 100% for each biologically
621 independent sample. Darker colored bars represent erythroid colonies (CFU-E) and lighter
622 colored bars represent granulocyte, erythrocyte, monocyte, macrophage (CFU-GEMM) colonies.
623 Plotted are means and SD of samples from n = 4 donors. Statistical significance was calculated
624 using 2-way ANOVA, and exact P-values are shown. **f**) Schematic of differentiation protocol
625 from HSCs to monocytes and subsequently to macrophages. **g**) Representative FACS analysis of
626 HSCs from BMR, BMY and HUCB at different stages of differentiation into the indicated cell
627 type, delineated by ovals. HSC are defined as $CD34^+CD38^-$, monocytes as $CD45^+CD14^+$, M1
628 macrophages as $CD45^+CD64^+$ and M2 macrophages as $CD45^+CD163^+$. **h**) Quantification of
629 FACS results from n=3 donors, where bars represent mean and SD of the percentage of the
630 indicated cell type.
631
632
633
634
635
636
637
638
639

FIGURE 3

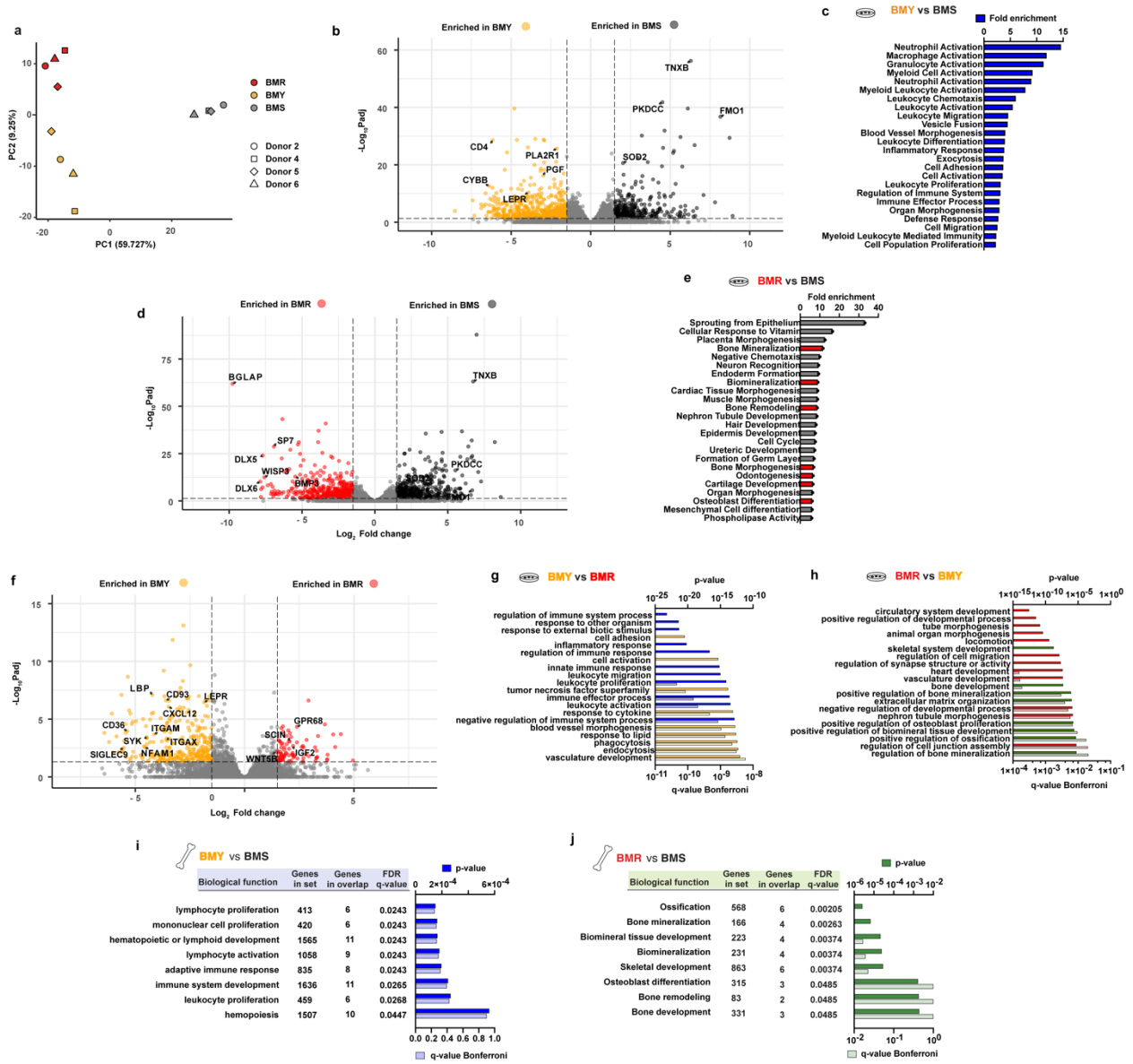

Fig. 3. Transcriptomic features of the human yellow and red bone marrow niches. Panels **a-h** are results from cells derived from BMS, BMY and BMR organoids cultured in mesenchymal media from n=4 subjects. Panels **i** and **j** are results from BMS, BMY and BMR tissue collected from n=2 subjects. **a**) Principal component analysis of differentially expressed genes between BMS vs (BMY + BMR) (n=4 human donors). **b**) Volcano plot of differentially expressed genes

647 between cells derived from BMY vs BMS organoids. **c**) Pathway enrichment analysis of genes
648 differentially expressed between cells derived from BMY compared to BMS. q-Bonferroni value
649 cut off <0.05 and fold change >2. **d**) Volcano plot of differentially expressed genes between cells
650 derived from BMR vs BMS organoids. **e**) Pathway enrichment analysis of genes differentially
651 expressed between cells derived from BMR compared to BMS. q-Bonferroni value cut off <0.05
652 and fold change >2. **f**) Volcano plot of differentially expressed genes between cells derived from
653 BMY vs BMR. **g**) Pathway enrichment analysis (GO: Biological Process) of genes more highly
654 expressed in BMY vs BMR. Immune system pathways are indicated in blue. **h**) Pathway
655 enrichment analysis (GO: Biological Process) of genes more highly expressed in BMR vs BMY.
656 Bone development pathways are indicated in green. **i-j**) Pathway enrichment analysis (GO:
657 Biological Process) of genes differentially expressed between BMY vs BMS (i) or BMR vs BMS
658 (j) tissues, selected from top 30 pathways.
659
660
661
662
663
664
665
666
667
668
669

670 **FIGURE 4**

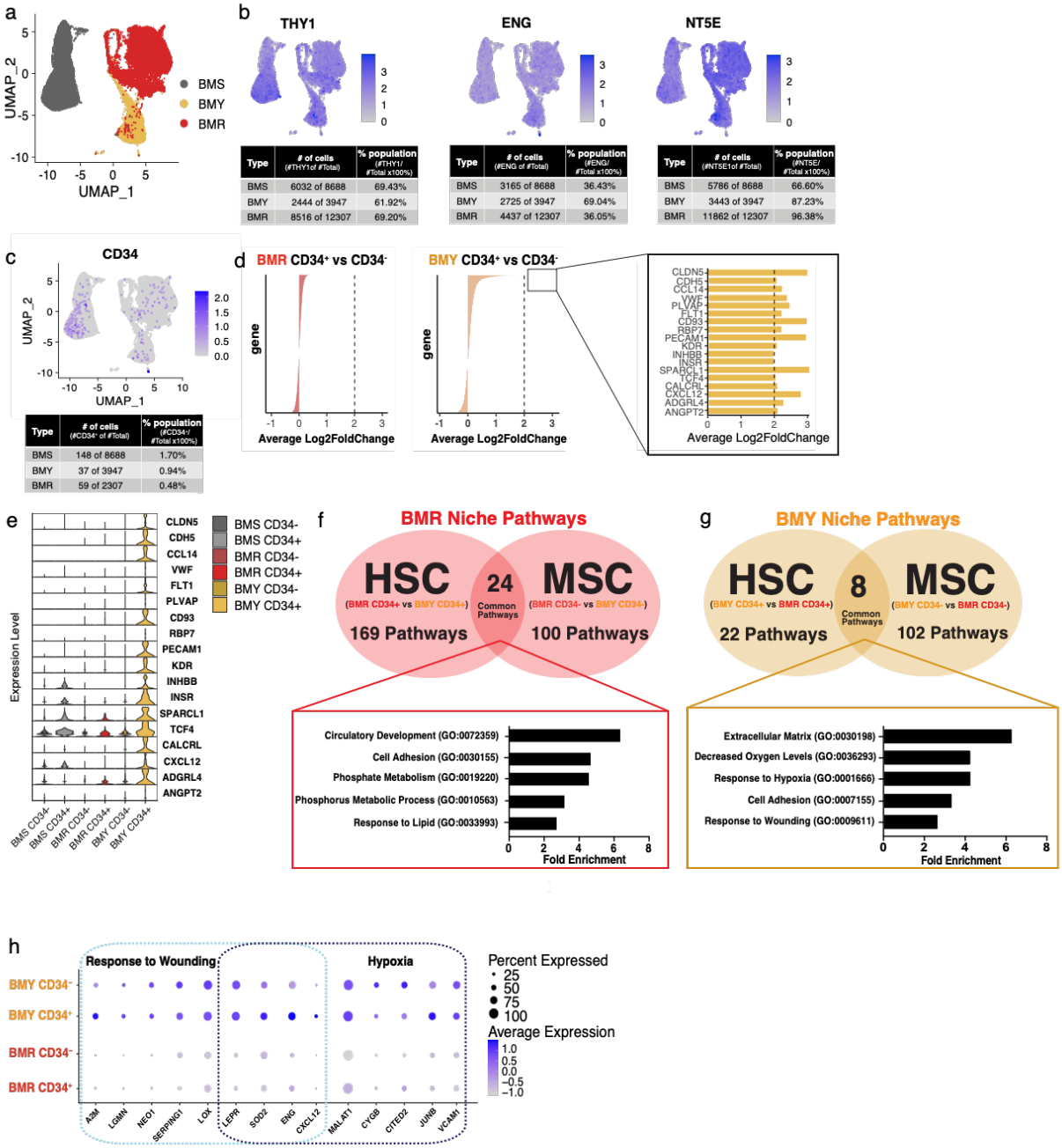

671

672 **Fig. 4. Distinct human HSC and mesenchymal progenitor cell populations derived from**

673 **BMY and BMR niches. a**) Dimensional reduction plot of single cell sequencing data, using

674 Uniform Manifold Approximation and Projection (UMAP), (n=1 human donor). **b**) Cells

675 expressing *THY1 (CD90), ENG (CD105),* and *NT5E (CD73)* mapped onto the UMAP

representation shown in (A) with cells expressing the indicated genes highlighted in purple. **c**) Cells expressing *CD34* mapped onto the UMAP representation shown in (a), with table below indicating number of $CD34^+$ cells in BMS, BMY, and BMR tissue depot with corresponding cell population percentages. **d**) Differential gene expresssion distribution between $CD34^+$ and $CD34^-$ cells derived from either BMR or BMY bone marrow niches. **e**) Violin plots of the top 18 genes differentially expressed between $CD34^+$ and $CD34^-$ cells in BMS, BMY, and BMR. **f**) Venn diagram identifying pathways characterizing the BMR niche, consisting in those pathways enriched by genes differentially expressed between BMY vs BMR using CD34+ (left) or CD34- cells (right). Pathways with q-Bonferroni value cut off <0.05 and fold change >2 are shown. **g**) Venn diagram identifying pathways characterizing the BMY niche, consisting in those pathways enriched by genes differentially expressed between BMY vs BMR using CD34+ (left) or CD34- cells (right). Pathways with q-Bonferroni value cut off <0.05 and fold change >2 are shown. **h**) Dot plot of genes expressed in $CD34^+$cells and $CD34^-$ cells derived from BMY and BMR that enrich the wounding (GO:0009611) or response to hypoxia (GO:0001666) pathways.

699 **FIGURE 5**

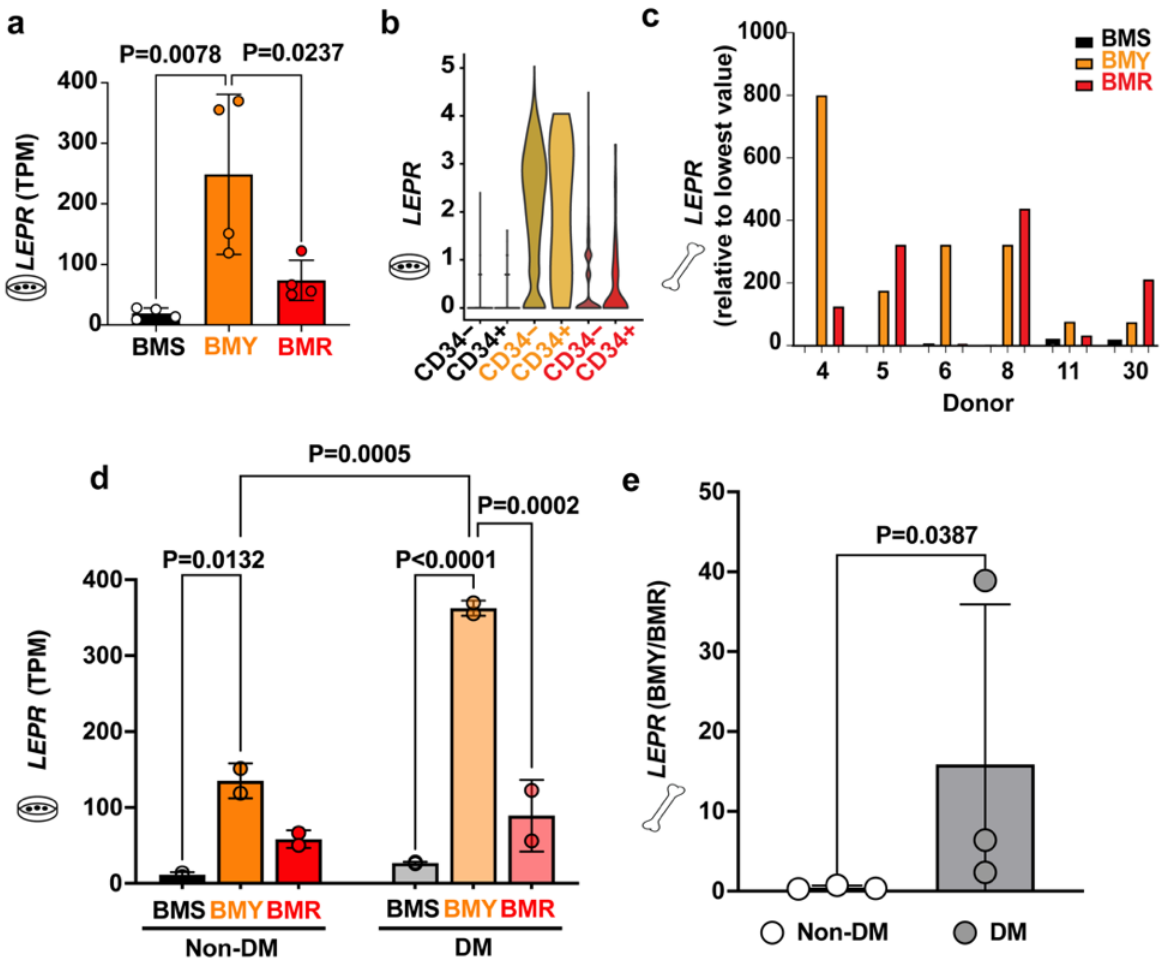

700

701 **Fig. 5. Leptin receptor in BMS, BMY and BMR tissue and tissue-derived cells. a**) Leptin
702 receptor (*LEPR*) expression derived from bulk RNASeq of cells from BMS, BMY and BMR.
703 Plotted are means and SD of values from n=4 donors. Statistical significance was calculated
704 using one-way ANOVA, and exact P values are indicated. **b**) Violin plot of *LEPR* expression in
705 single cells from BMR, BMY, and BMS from a single donor. **c**) *LEPR* expression determined by
706 RT-PCR from BMS, BMY, and BMR tissue excised from n=6 donors. Bars represent the mean
707 and SD relative to lowest value in the dataset. **d**) Leptin receptor (*LEPR*) expression values
708 derived from bulk RNASeq of cells expanded from BMS, BMY and BMR from donors with no
709 diabetes (Non-DM) or diabetes (DM). Bars are means and SD from n=2 Non-DM and 2 DM.

710 Statistical significance was calculated using two-way ANOVA. **e**) *LEPR* expression determined
711 by RT-PCR from BMY and BMR tissue excised from donors with or without diabetes. Data
712 points are the ratio of values in BMY/BMR for each subject. Bars are means and SD of n=3
713 donors for Non-DM and n=3 donors for DM groups. Exact P values are shown.
714
715
716 **DECLARATION OF INTERESTS**
717 The authors declare no competing interests.
718
719
720 **REFERENCES**
721

722 1 Kricun, M. E. Red-yellow marrow conversion: its effect on the location of some solitary
723 bone lesions. *Skeletal Radiol* **14**, 10-19, doi:10.1007/BF00361188 (1985).
724 2 Moore, S. G. & Dawson, K. L. Red and yellow marrow in the femur: age-related changes
725 in appearance at MR imaging. *Radiology* **175**, 219-223,
726 doi:10.1148/radiology.175.1.2315484 (1990).
727 3 Ambrosi, T. H. & Schulz, T. J. The emerging role of bone marrow adipose tissue in bone
728 health and dysfunction. *J Mol Med (Berl)* **95**, 1291-1301, doi:10.1007/s00109-017-1604-
729 7 (2017).
730 4 Ferraro, F. *et al.* Diabetes impairs hematopoietic stem cell mobilization by altering niche
731 function. *Sci Transl Med* **3**, 104ra101, doi:10.1126/scitranslmed.3002191 (2011).

732 5 Krings, A. *et al.* Bone marrow fat has brown adipose tissue characteristics, which are
733 attenuated with aging and diabetes. *Bone* **50**, 546-552, doi:10.1016/j.bone.2011.06.016
734 (2012).
735 6 Lecka-Czernik, B. Marrow fat metabolism is linked to the systemic energy metabolism.
736 *Bone* **50**, 534-539, doi:10.1016/j.bone.2011.06.032 (2012).
737 7 Luo, L. G., Xiong, F., Ravassard, P. & Luo, J. Z. Human Bone Marrow Subpopulations
738 Sustain Human Islet Function and Viability In vitro. *Br J Med Med Res* **8**, 576-587,
739 doi:10.9734/BJMMR/2015/17536 (2015).
740 8 van den Berg, S. M. *et al.* Diet-induced obesity in mice diminishes hematopoietic stem
741 and progenitor cells in the bone marrow. *FASEB J* **30**, 1779-1788,
742 doi:10.1096/fj.201500175 (2016).
743 9 Sebo, Z. L. *et al.* Bone Marrow Adiposity: Basic and Clinical Implications. *Endocr Rev*
744 **40**, 1187-1206, doi:10.1210/er.2018-00138 (2019).
745 10 Beerman, I. *et al.* Functionally distinct hematopoietic stem cells modulate hematopoietic
746 lineage potential during aging by a mechanism of clonal expansion. *Proc Natl Acad Sci U*
747 *S A* **107**, 5465-5470, doi:10.1073/pnas.1000834107 (2010).
748 11 Kuranda, K. *et al.* Age-related changes in human hematopoietic stem/progenitor cells.
749 *Aging Cell* **10**, 542-546, doi:10.1111/j.1474-9726.2011.00675.x (2011).
750 12 Li, X. *et al.* Mechanisms and rejuvenation strategies for aged hematopoietic stem cells. *J*
751 *Hematol Oncol* **13**, 31, doi:10.1186/s13045-020-00864-8 (2020).
752 13 Morrison, S. J., Wandycz, A. M., Akashi, K., Globerson, A. & Weissman, I. L. The aging
753 of hematopoietic stem cells. *Nat Med* **2**, 1011-1016, doi:10.1038/nm0996-1011 (1996).

754 14 Pang, W. W., Schrier, S. L. & Weissman, I. L. Age-associated changes in human
755 hematopoietic stem cells. *Semin Hematol* **54**, 39-42,
756 doi:10.1053/j.seminhematol.2016.10.004 (2017).
757 15 Kovtonyuk, L. V., Fritsch, K., Feng, X., Manz, M. G. & Takizawa, H. Inflamm-Aging of
758 Hematopoiesis, Hematopoietic Stem Cells, and the Bone Marrow Microenvironment.
759 *Front Immunol* **7**, 502, doi:10.3389/fimmu.2016.00502 (2016).
760 16 Sioud, M., Floisand, Y., Forfang, L. & Lund-Johansen, F. Signaling through toll-like
761 receptor 7/8 induces the differentiation of human bone marrow CD34+ progenitor cells
762 along the myeloid lineage. *J Mol Biol* **364**, 945-954, doi:10.1016/j.jmb.2006.09.054
763 (2006).
764 17 Laharrague, P. *et al.* High concentration of leptin stimulates myeloid differentiation from
765 human bone marrow CD34+ progenitors: potential involvement in leukocytosis of obese
766 subjects. *Int J Obes Relat Metab Disord* **24**, 1212-1216, doi:10.1038/sj.ijo.0801377
767 (2000).
768 18 Singer, K. *et al.* Diet-induced obesity promotes myelopoiesis in hematopoietic stem cells.
769 *Mol Metab* **3**, 664-675, doi:10.1016/j.molmet.2014.06.005 (2014).
770 19 Rojas-Rodriguez, R. *et al.* Generation of Functional Human Adipose Tissue in Mice from
771 Primed Progenitor Cells. *Tissue Eng Part A* **25**, 842-854,
772 doi:10.1089/ten.TEA.2018.0067 (2019).
773 20 Min, S. Y. *et al.* Human 'brite/beige' adipocytes develop from capillary networks, and
774 their implantation improves metabolic homeostasis in mice. *Nat Med* **22**, 312-318,
775 doi:10.1038/nm.4031 (2016).

776 21 Rojas-Rodriguez, R. *et al.* Adipose tissue angiogenesis assay. *Methods Enzymol* **537**, 75-
777 91, doi:10.1016/B978-0-12-411619-1.00005-7 (2014).
778 22 Min, S. Y. *et al.* Diverse repertoire of human adipocyte subtypes develops from
779 transcriptionally distinct mesenchymal progenitor cells. *Proc Natl Acad Sci U S A* **116**,
780 17970-17979, doi:10.1073/pnas.1906512116 (2019).
781 23 Tratwal, J., Rojas-Sutterlin, S., Bataclan, C., Blum, S. & Naveiras, O. Bone marrow
782 adiposity and the hematopoietic niche: A historical perspective of reciprocity,
783 heterogeneity, and lineage commitment. *Best Pract Res Clin Endocrinol Metab* **35**,
784 101564, doi:10.1016/j.beem.2021.101564 (2021).
785 24 Naveiras, O. *et al.* Bone-marrow adipocytes as negative regulators of the haematopoietic
786 microenvironment. *Nature* **460**, 259-263, doi:10.1038/nature08099 (2009).
787 25 Tao, L., Togarrati, P. P., Choi, K. D. & Suknuntha, K. StemRegenin 1 selectively
788 promotes expansion of Multipotent Hematopoietic Progenitors derived from Human
789 Embryonic Stem Cells. *J Stem Cells Regen Med* **13**, 75-79 (2017).
790 26 Fares, I. *et al.* Cord blood expansion. Pyrimidoindole derivatives are agonists of human
791 hematopoietic stem cell self-renewal. *Science* **345**, 1509-1512,
792 doi:10.1126/science.1256337 (2014).
793 27 Tajer, P., Pike-Overzet, K., Arias, S., Havenga, M. & Staal, F. J. T. Ex Vivo Expansion
794 of Hematopoietic Stem Cells for Therapeutic Purposes: Lessons from Development and
795 the Niche. *Cells* **8**, doi:10.3390/cells8020169 (2019).
796 28 Schnyder, T. *et al.* B cell receptor-mediated antigen gathering requires ubiquitin ligase
797 Cbl and adaptors Grb2 and Dok-3 to recruit dynein to the signaling microcluster.
798 *Immunity* **34**, 905-918, doi:10.1016/j.immuni.2011.06.001 (2011).

799 29 Nolin, J. D. *et al.* Identification of Epithelial Phospholipase A(2) Receptor 1 as a
800 Potential Target in Asthma. *Am J Respir Cell Mol Biol* **55**, 825-836,
801 doi:10.1165/rcmb.2015-0150OC (2016).
802 30 Tsukumo, S., Hirose, K., Maekawa, Y., Kishihara, K. & Yasutomo, K. Lunatic fringe
803 controls T cell differentiation through modulating notch signaling. *J Immunol* **177**, 8365-
804 8371, doi:10.4049/jimmunol.177.12.8365 (2006).
805 31 Luttun, A., Tjwa, M. & Carmeliet, P. Placental growth factor (PlGF) and its receptor Flt-
806 1 (VEGFR-1): novel therapeutic targets for angiogenic disorders. *Ann N Y Acad Sci* **979**,
807 80-93, doi:10.1111/j.1749-6632.2002.tb04870.x (2002).
808 32 De Ravin, S. S. *et al.* CRISPR-Cas9 gene repair of hematopoietic stem cells from patients
809 with X-linked chronic granulomatous disease. *Sci Transl Med* **9**,
810 doi:10.1126/scitranslmed.aah3480 (2017).
811 33 Trinh, T. *et al.* Leptin receptor, a surface marker for a subset of highly engrafting long-
812 term functional hematopoietic stem cells. *Leukemia* **35**, 2064-2075, doi:10.1038/s41375-
813 020-01079-z (2021).
814 34 Comazzetto, S. *et al.* Restricted Hematopoietic Progenitors and Erythropoiesis Require
815 SCF from Leptin Receptor+ Niche Cells in the Bone Marrow. *Cell Stem Cell* **24**, 477-486
816 e476, doi:10.1016/j.stem.2018.11.022 (2019).
817 35 Sugiyama, T., Omatsu, Y. & Nagasawa, T. Niches for hematopoietic stem cells and
818 immune cell progenitors. *Int Immunol* **31**, 5-11, doi:10.1093/intimm/dxy058 (2019).
819 36 Zhou, B. O. *et al.* Bone marrow adipocytes promote the regeneration of stem cells and
820 haematopoiesis by secreting SCF. *Nat Cell Biol* **19**, 891-903, doi:10.1038/ncb3570
821 (2017).

822 37 Samee, N. *et al.* Dlx5, a positive regulator of osteoblastogenesis, is essential for
823 osteoblast-osteoclast coupling. *Am J Pathol* **173**, 773-780,
824 doi:10.2353/ajpath.2008.080243 (2008).
825 38 Wang, J. S. *et al.* Control of osteocyte dendrite formation by Sp7 and its target gene
826 osteocrin. *Nat Commun* **12**, 6271, doi:10.1038/s41467-021-26571-7 (2021).
827 39 Daluiski, A. *et al.* Bone morphogenetic protein-3 is a negative regulator of bone density.
828 *Nat Genet* **27**, 84-88, doi:10.1038/83810 (2001).
829 40 Kutz, W. E., Gong, Y. & Warman, M. L. WISP3, the gene responsible for the human
830 skeletal disease progressive pseudorheumatoid dysplasia, is not essential for skeletal
831 function in mice. *Mol Cell Biol* **25**, 414-421, doi:10.1128/MCB.25.1.414-421.2005
832 (2005).
833 41 Gao, S. *et al.* Identification of HSC/MPP expansion units in fetal liver by single-cell
834 spatiotemporal transcriptomics. *Cell Res* **32**, 38-53, doi:10.1038/s41422-021-00540-7
835 (2022).
836 42 Iwasaki, M., Liedtke, M., Gentles, A. J. & Cleary, M. L. CD93 Marks a Non-Quiescent
837 Human Leukemia Stem Cell Population and Is Required for Development of MLL-
838 Rearranged Acute Myeloid Leukemia. *Cell Stem Cell* **17**, 412-421,
839 doi:10.1016/j.stem.2015.08.008 (2015).
840 43 Kinstrie, R. *et al.* CD93 is expressed on chronic myeloid leukemia stem cells and
841 identifies a quiescent population which persists after tyrosine kinase inhibitor therapy.
842 *Leukemia* **34**, 1613-1625, doi:10.1038/s41375-019-0684-5 (2020).

843 44 Pessoa Rodrigues, C. & Akhtar, A. Differential H4K16ac levels ensure a balance
844 between quiescence and activation in hematopoietic stem cells. *Sci Adv* **7**,
845 doi:10.1126/sciadv.abi5987 (2021).
846 45 Knapp, S., de Vos, A. F., Florquin, S., Golenbock, D. T. & van der Poll, T.
847 Lipopolysaccharide binding protein is an essential component of the innate immune
848 response to Escherichia coli peritonitis in mice. *Infect Immun* **71**, 6747-6753,
849 doi:10.1128/IAI.71.12.6747-6753.2003 (2003).
850 46 Maryanovich, M. & Ito, K. CD36-Mediated Fatty Acid Oxidation in Hematopoietic Stem
851 Cells Is a Novel Mechanism of Emergency Hematopoiesis in Response to Infection.
852 *Immunometabolism* **4**, doi:10.20900/immunometab20220008 (2022).
853 47 Mistry, J. J. *et al.* Free fatty-acid transport via CD36 drives beta-oxidation-mediated
854 hematopoietic stem cell response to infection. *Nat Commun* **12**, 7130,
855 doi:10.1038/s41467-021-27460-9 (2021).
856 48 Wang, L. *et al.* Gain-of-function variants in SYK cause immune dysregulation and
857 systemic inflammation in humans and mice. *Nat Genet* **53**, 500-510, doi:10.1038/s41588-
858 021-00803-4 (2021).
859 49 Prashad, S. L. *et al.* GPI-80 defines self-renewal ability in hematopoietic stem cells
860 during human development. *Cell Stem Cell* **16**, 80-87, doi:10.1016/j.stem.2014.10.020
861 (2015).
862 50 Hou, L., Voit, R. A., Sankaran, V. G., Springer, T. A. & Yuki, K. CD11c regulates
863 hematopoietic stem and progenitor cells under stress. *Blood Adv* **4**, 6086-6097,
864 doi:10.1182/bloodadvances.2020002504 (2020).

865 51 Biedermann, B., Gil, D., Bowen, D. T. & Crocker, P. R. Analysis of the CD33-related
866 siglec family reveals that Siglec-9 is an endocytic receptor expressed on subsets of acute
867 myeloid leukemia cells and absent from normal hematopoietic progenitors. *Leuk Res* **31**,
868 211-220, doi:10.1016/j.leukres.2006.05.026 (2007).
869 52 Ohtsuka, M. *et al.* NFAM1, an immunoreceptor tyrosine-based activation motif-bearing
870 molecule that regulates B cell development and signaling. *Proc Natl Acad Sci U S A* **101**,
871 8126-8131, doi:10.1073/pnas.0401119101 (2004).
872 53 Sugiyama, T., Kohara, H., Noda, M. & Nagasawa, T. Maintenance of the hematopoietic
873 stem cell pool by CXCL12-CXCR4 chemokine signaling in bone marrow stromal cell
874 niches. *Immunity* **25**, 977-988, doi:10.1016/j.immuni.2006.10.016 (2006).
875 54 Zhang, J. *et al.* Identification of the haematopoietic stem cell niche and control of the
876 niche size. *Nature* **425**, 836-841, doi:10.1038/nature02041 (2003).
877 55 Baumann, C. I. *et al.* PECAM-1 is expressed on hematopoietic stem cells throughout
878 ontogeny and identifies a population of erythroid progenitors. *Blood* **104**, 1010-1016,
879 doi:10.1182/blood-2004-03-0989 (2004).
880 56 Ross, E. A. *et al.* A novel role for PECAM-1 (CD31) in regulating haematopoietic
881 progenitor cell compartmentalization between the peripheral blood and bone marrow.
882 *PLoS One* **3**, e2338, doi:10.1371/journal.pone.0002338 (2008).
883 57 Baryawno, N. *et al.* A Cellular Taxonomy of the Bone Marrow Stroma in Homeostasis
884 and Leukemia. *Cell* **177**, 1915-1932 e1916, doi:10.1016/j.cell.2019.04.040 (2019).
885 58 Jalili, A., Shirvaikar, N., Marquez-Curtis, L. A., Turner, A. R. & Janowska-Wieczorek,
886 A. The HGF/c-Met axis synergizes with G-CSF in the mobilization of hematopoietic
887 stem/progenitor cells. *Stem Cells Dev* **19**, 1143-1151, doi:10.1089/scd.2009.0376 (2010).

888 59 Cao, H. *et al.* Osteopontin is An Important Regulative Component of the Fetal Bone
889 Marrow Hematopoietic Stem Cell Niche. *Cells* **8**, doi:10.3390/cells8090985 (2019).
890 60 Guidi, N. *et al.* Osteopontin attenuates aging-associated phenotypes of hematopoietic
891 stem cells. *EMBO J* **36**, 840-853, doi:10.15252/embj.201694969 (2017).
892 61 Li, J. *et al.* Murine hematopoietic stem cell reconstitution potential is maintained by
893 osteopontin during aging. *Sci Rep* **8**, 2833, doi:10.1038/s41598-018-21324-x (2018).
894 62 Buono, M., Visigalli, I., Bergamasco, R., Biffi, A. & Cosma, M. P. Sulfatase modifying
895 factor 1-mediated fibroblast growth factor signaling primes hematopoietic multilineage
896 development. *J Exp Med* **207**, 1647-1660, doi:10.1084/jem.20091022 (2010).
897 63 Gadomski, S. *et al.* Id1 and Id3 Maintain Steady-State Hematopoiesis by Promoting
898 Sinusoidal Endothelial Cell Survival and Regeneration. *Cell Rep* **31**, 107572,
899 doi:10.1016/j.celrep.2020.107572 (2020).
900 64 Bennett, B. D. *et al.* A role for leptin and its cognate receptor in hematopoiesis. *Curr Biol*
901 **6**, 1170-1180, doi:10.1016/s0960-9822(02)70684-2 (1996).
902 65 Claycombe, K., King, L. E. & Fraker, P. J. A role for leptin in sustaining lymphopoiesis
903 and myelopoiesis. *Proc Natl Acad Sci U S A* **105**, 2017-2021,
904 doi:10.1073/pnas.0712053105 (2008).
905 66 Fernandez-Riejos, P. *et al.* Role of leptin in the activation of immune cells. *Mediators*
906 *Inflamm* **2010**, 568343, doi:10.1155/2010/568343 (2010).
907 67 Laharrague, P. *et al.* High expression of leptin by human bone marrow adipocytes in
908 primary culture. *FASEB J* **12**, 747-752, doi:10.1096/fasebj.12.9.747 (1998).
909 68 Umemoto, Y. *et al.* Leptin stimulates the proliferation of murine myelocytic and
910 primitive hematopoietic progenitor cells. *Blood* **90**, 3438-3443 (1997).

911 69 Botolin, S. & McCabe, L. R. Bone loss and increased bone adiposity in spontaneous and
912 pharmacologically induced diabetic mice. *Endocrinology* **148**, 198-205,
913 doi:10.1210/en.2006-1006 (2007).
914 70 Esplin, B. L. *et al.* Chronic exposure to a TLR ligand injures hematopoietic stem cells. *J*
915 *Immunol* **186**, 5367-5375, doi:10.4049/jimmunol.1003438 (2011).
916 71 Mann, M. *et al.* Heterogeneous Responses of Hematopoietic Stem Cells to Inflammatory
917 Stimuli Are Altered with Age. *Cell Rep* **25**, 2992-3005 e2995,
918 doi:10.1016/j.celrep.2018.11.056 (2018).
919 72 Yan, J. *et al.* Diabetes impairs wound healing by Dnmt1-dependent dysregulation of
920 hematopoietic stem cells differentiation towards macrophages. *Nat Commun* **9**, 33,
921 doi:10.1038/s41467-017-02425-z (2018).
922 73 Mantel, C. R. *et al.* Enhancing Hematopoietic Stem Cell Transplantation Efficacy by
923 Mitigating Oxygen Shock. *Cell* **161**, 1553-1565, doi:10.1016/j.cell.2015.04.054 (2015).
924 74 Yukselen, O., Turkyilmaz, O., Ozturk, A. R., Garber, M. & Kucukural, A. DolphinNext:
925 a distributed data processing platform for high throughput genomics. *BMC Genomics* **21**,
926 310, doi:10.1186/s12864-020-6714-x (2020).
927 75 Li, B. & Dewey, C. N. RSEM: accurate transcript quantification from RNA-Seq data
928 with or without a reference genome. *BMC Bioinformatics* **12**, 323, doi:10.1186/1471-
929 2105-12-323 (2011).
930 76 Kucukural, A., Yukselen, O., Ozata, D. M., Moore, M. J. & Garber, M. DEBrowser:
931 interactive differential expression analysis and visualization tool for count data. *BMC*
932 *Genomics* **20**, 6, doi:10.1186/s12864-018-5362-x (2019).

933 77 Hao, Y. *et al.* Integrated analysis of multimodal single-cell data. *Cell* **184**, 3573-3587
934 e3529, doi:10.1016/j.cell.2021.04.048 (2021).
935